RSC Sustainability

ROYAL SOCIETY OF CHEMISTRY

PAPER

View Article Online
View Journal

Cite this: DOI: 10.1039/d5su00687b

Spent coffee ground-derived biochar with trimodal porosity: green biochar supported highly dispersed TiO_2 and Nb_2O_5 nanoparticles as an efficient novel catalyst for lactic acid synthesis

Vlad A. Neacșu, †[a] Maria Minodora Marin,†[a] Anca Dumitru,[b] Cristina Elena Stavarache,[ac] Elena Olăreț,[a] Erika Blânzeanu,[a] Dana Culiță,[d] Victor Fruth,[d] Florica Papa,[d] Marielle Huvé,[e] Pascal Granger *[e] and Marian Nicolae Verziu *[a]

Received 19th August 2025
Accepted 4th November 2025

DOI: 10.1039/d5su00687b

rsc.li/rscsus

Lactic acid obtained from cellulose over heterogeneous acid catalysts is one of the key areas in bioeconomy. Herein, we develop a series of biochar-supported nano-titanium–niobium oxides (with 10% Ti and 0.25 to 15% Nb) prepared *via* wet impregnation and evaluate their performances in cellulose conversion to lactic acid. We report for the first time a biochar which displays trimodal (micro-, meso-, and macro-) porosity and high surface area due to the synergistic effect between lanthanum and zinc during the carbonization of spent coffee grounds. The successful impregnation of Nb and Ti species on the surface of the biochar was confirmed by XRD, TGA, XPS, AFM, SEM-EDS, and STEM-EDS. The presence of niobia and titania generated a significant increase in the catalyst's acidity as noticed by NH_3-TPD and, subsequently, improved the lactic acid yield from 1.6% (for 10% Ti/AC) to 14% (for 10% Ti–0.5% Nb/AC). Furthermore, the high-water tolerance of niobium and titanium species allowed the biochar-supported nano-titanium–niobium oxides to be recycled three times without a significant loss in their catalytic activity.

Sustainability spotlight

This study focuses on the valorisation of spent coffee grounds into a green biochar, with trimodal porosity, which supports highly dispersed TiO_2 and Nb_2O_5 nanoparticles and is used for the conversion of cellulose to value-added compounds such as lactic acid. Both the synthesis of these new materials and lactic production from cellulose were carried out in agreement with the principles of green chemistry. Therefore, this work aligns with the United Nations Sustainable Development Goals mainly with responsible consumption and production (SDG 12) and climate action (SDG 13).

1 Introduction

The negative environmental impact of using fossil resources encouraged the transition to renewable resources and the implementation of the circular economy strategy by producing value-added compounds to address the climate change issues.[1,2] Cellulose aligns with the principle of the circular economy, being the most abundant natural polymer on the planet and an inedible renewable resource.[3]

The linear structure of cellulose, which involves glucose units connected through β-1,4-glycosidic bonds, becomes an important target for industry in view of its transformation into value-added products such as ethylene glycol,[4] 5-hydroxymethylfurfural (HMF),[5] levulinic acid (LevA),[6] lactic acid (2-hydroxypropanoic acid, LacA),[7,8] or glycolic acid (GlycA).[9] Among them, LacA is one of the most important platform molecules due to its wide applications in food processing and preservation, the pharmaceutical and cosmetic industries,[10] and the production of other bio-based chemicals (*e.g.*, acrylic acid, 2,3-pentanedione, and acetaldehyde).[7] The catalytic system involved in the reaction, whether a base, a Lewis acid, or a redox perovskite, is one of the key challenges for the efficient conversion of cellulose and cellulose-derived carbohydrates to

[a]*Department of Bioresources and Polymer Science, Advanced Polymer Materials Group, Faculty of Chemical Engineering and Biotechnologies, National University of Science and Technology Politehnica Bucharest, 1-7 Gh. Polizu Street, Bucharest, Romania. E-mail: marian.verziu@upb.ro*

[b]*Faculty of Physics, University of Bucharest, 077125 Măgurele, Romania*

[c]*"C.D. Nenițescu" Institute of Organic and Supramolecular Chemistry, 202-B Splaiul Independenței, RO-060023, Bucharest, Romania*

[d]*"Ilie Murgulescu" Institute of Physical Chemistry, Romanian Academy, Bucharest, 060021, Romania*

[e]*Univ. Lille, CNRS, Centrale Lille, Univ. Artois, UMR 8181 – UCCS – Unité de Catalyse et Chimie du Solide, F-59000 Lille, France. E-mail: pascal.granger@univ-lille.fr*

† Both authors contributed equally.

LacA. Compared to alkali (producing mainly lactates) or perovskites (LacA yield < 50%), the LacA yields (η_{LacA}) from carbohydrates obtained on Lewis acid catalysts are higher than 50%.[11] The transformation of cellulose into LacA involves both Brønsted and Lewis acid sites and is carried out in several steps (Scheme 1): Brønsted acid sites catalyse the hydrolysis of cellulose to glucose, which then isomerises to fructose. Fructose undergoes a retro-aldol reaction over Lewis acid sites and is converted to 1,3-dihydroxyacetone and glyceraldehyde, with the latter then being converted to LacA.[12,13]

LacA production from biomass at industrial scale is not feasible without lowering the costs and increasing the efficiency of catalysts. The use of alkaline catalysts such as $Ca(OH)_2$ in the conversion of cellulose led to a high η_{LacA} (~27%) in a short time (90 s),[14] but further developments were limited by the poor recyclability of the catalyst and the undesired reaction between the catalyst and LacA, resulting in calcium lactate. In the search for cheap and efficient catalysts, a particular interest has been paid to developing heterogeneous catalysts, due to their facile recovery and improved recyclability. Alumina-supported catalysts with various amounts of erbium oxide showed good catalytic activity in the one-pot conversion of cellulose to LacA in aqueous solution under an inert atmosphere and the highest η_{LacA} (45.8% in 3 h) was obtained at 240 °C.[15] Zhang *et al.*[16] studied the influence of Zn, Ni, and activated carbon in the presence of NaOH on the hydrothermal conversion of glucose to LacA. The large surface area of activated carbon, which increased the contact area of the reactants, and the presence of Zn and Ni improved the production of LacA, reaching η_{LacA} up to 55%. The importance of Lewis acid sites of Sn–beta zeolites was also highlighted by Holm *et al.*[17] in the production of LacA or its derivatives from carbohydrates. The addition of Mg besides Sn in beta zeolites led to a higher η_{LacA} from biomass-derived carbohydrates due to the synergistic effects of bimetals and the hierarchical structures in Mg–Sn–beta-H zeolites.[18] η_{LacA} above 50% was also reported by Cui *et al.*[19] in the conversion of glucose over hierarchical Zr–BEA zeolites. Moreover, the cooccurrence of Lewis and mild Brønsted acidity of ZrO_2–TiO_2 (ref. 20) or porous titanosilicates[21] allowed the production of lactates from trioses. On the other hand, the poisoning of acid sites by water narrowed down the applicability of solid acids in the aqueous medium.[22] Alternative approaches investigated the use of Nb-based catalysts in various biomass-derivative conversions, due to the high stability of their acid sites in aqueous media. Both Lewis and Brønsted acid sites coexist at the surface of Nb_2O_5, but the incorporation of Sn enhanced the Lewis acidity and consequently the η_{LacA} (up to 83%).[23] Thus, the catalytic performances of Nb-based materials ($Nb@CaF_2$ $Nb@AlF_3$) in the conversion of cellulose to LacA were previously studied and it was found that η_{LacA} is directly correlated with the niobium content in niobium-modified aluminium hydroxyfluorides ($Nb@Al(OH)_xF_{3-x}$), while $Nb@Ca(OH)_xF_{2-x}$ catalysts displayed improved hydrothermal stability and led to similar yields (15.4% over $Nb@Ca(OH)_xF_{2-x}$ *versus* 17.0% over $Nb@Al(OH)_xF_{3-x}$).[24,25]

Herein we report the synthesis of nano-Ti- and Nb-based catalysts with high stability and surface area after deposition on a new mesoporous activated biochar (AC) prepared from spent coffee grounds (SCGs). AC offers enhanced dispersion, improved durability and reusability of the catalysts, and provides a stable framework that minimises catalyst leaching.[26] In this study, we converted SCGs to a biochar by carbonising them together with appropriate amounts of zinc and lanthanum chloride. For the first time, we obtained a biochar with both micro- and mesopores and a high surface area. These characteristics are particularly interesting since the activation with $FeCl_3$,[27] $ZnCl_2$,[28] or KOH[29] led to biochars with high surface area, but much smaller pores compared to those reported in this work. Moreover, the ability to create catalytically-active metal sites with precise dimensions, distribution, and positioning in micro-, meso-, and macroporous materials also caught the attention of researchers from industry and academia. One application of these new materials was their catalytic performance in the conversion of cellulose to LacA, where the titania-based catalyst shows low catalytic performances.[30] Different parameters of the catalyst were investigated, including niobium content, textural properties, and the reaction conditions, especially the temperature as a critical parameter for kinetics and stability.

2 Experimental section

2.1. Materials

The National University of Science and Technology Politehnica Bucharest cafeteria provided the SCGs. Lanthanum(III) chloride ($LaCl_3 \cdot 7H_2O$) and zinc(II) chloride ($ZnCl_2$) were purchased from VWR Chemicals. Hydrochloric acid (HCl 35%) and nitric acid (HNO_3 65%) were purchased from Supelco. α-Cellulose, ammonium niobate(V) oxalate hydrate and titanium(IV) bis(ammonium lactato)dihydroxide (solution 50%) were purchased from Sigma-Aldrich.

All reagents were used as received, without further purification.

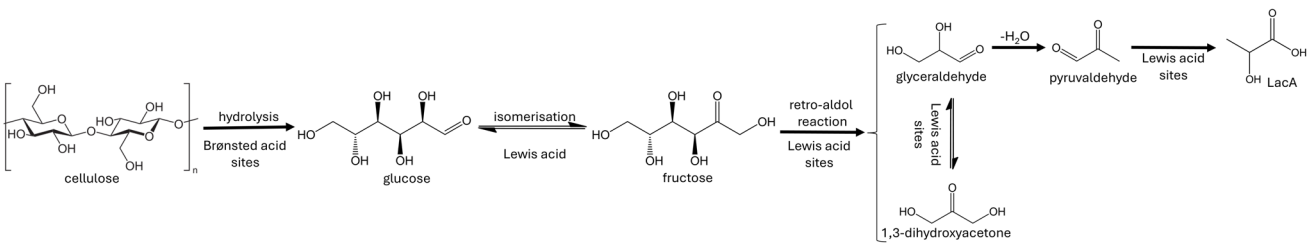

Scheme 1 Suggested mechanism for the formation of LacA from cellulose.

2.2. Catalyst preparation

2.2.1. Activated biochar synthesis. The mesoporous activated biochar (AC) was prepared as described by Verziu *et al.*[31] with slight modifications. For a detailed description of the synthesis, see Note S1.

For comparison, two other biochars were synthesised, but they were activated with either only $ZnCl_2$ (AC_{micro}) or $LaCl_3$ (AC_{LaCl_3}).

2.2.2. Preparation of activated biochar supported titanium and niobium. The anchoring of titanium and niobium on the surface of AC by wet impregnation was carried out as follows: 1 g AC was suspended in 15 mL water and then titanium(IV) bis(ammonium lactato)dihydroxide solution and ammonium niobate(V) oxalate hydrate were added under stirring at room temperature for 6 h with adjusted amounts in order to obtain 10% Ti/AC, 10% Ti–0.25% Nb/AC, 10% Ti–0.5% Nb/AC, 10% Ti–1% Nb/AC, 10% Ti–3% Nb/AC, 10% Ti–10% Nb/AC, and 10% Ti–15% Nb/AC. The resulting materials were dried at 100 °C and calcined at 500 °C for 1 h under nitrogen flow. The calcination temperature was not increased any further to avoid the phase transformation of anatase into rutile (between 500 and 600 °C (ref. 32)), since anatase shows a higher catalytic activity compared to rutile in catalytic glucose conversion.[33]

For comparison, the AC_{micro} was further impregnated with titanium and niobium in order to obtain 10% Ti–10% Nb/AC_{micro}.

2.3. Characterisation techniques

The textural properties were characterised using nitrogen adsorption/desorption isotherms. The acidity was determined by ammonia temperature-programmed desorption (NH_3-TPD). The structural properties were investigated by powder X-ray diffraction (PXRD), X-ray photoelectron spectroscopy (XPS), atomic force microscopy (AFM), scanning electron microscopy-energy dispersive X-ray spectroscopy (SEM-EDS) and high-resolution scanning transmission electron microscopy (HR-STEM). Thermal decomposition was investigated through thermogravimetric analysis. For more information on the characterisation techniques, refer to Note S1.

2.4. Catalytic testing

Cellulose conversion to LacA was performed under autoclave conditions at 180 °C or 210 °C for 24 h under vigorous stirring according to the following protocol: a solution of 0.5 g cellulose in 20 mL water was added over 0.1 or 0.2 g of catalyst. After the reaction, the catalyst was recovered by centrifugation.

For the catalytic stability tests, the recovered mixture (catalyst and unreacted cellulose) was washed with water, dried, and weighed. Then a fresh amount of cellulose equal to the amount of reacted cellulose was added in order to evaluate the catalytic activity using the same experimental conditions that were used in the first catalytic cycle. The reaction products (Fig. S1) were analysed by GC-FID using an 8890GC System Agilent, HP-5MS inert column (30 m × 0.25 mm ID × 0.25 μm film). The carrier gas used is helium with a flow of 1 mL min^{-1}, the injector was operated at 280 °C with a split ratio of 100 : 1 and the oven temperature was programmed as follows: 60 °C for 1 min and then gradually increased to 280 °C at 10 °C min^{-1}. The identification of the silylated derivatives of water-soluble products was made using an 8890 GC System Agilent gas chromatograph equipped with a 5977C GC/MSD mass spectrometer using the aforementioned conditions. The procedure used in chromatographic analysis was similar to that reported in our previous study.[34]

3 Results and discussion

3.1. Material characterisation

The XRD patterns of the AC-supported titanium and/or niobium reflect amorphous materials with broad reflections appearing at $2\theta = 25.4°$, 37.8°, 48.5°, 54°, 55.4°, and 62.9° (Fig. 1a), which are characteristic of the (101), (004), (200), (105), (211), and (204) planes of anatase TiO_2, respectively.[35] Typical reflections for Nb_2O_5 expected at $2\theta = 22.6°$, 28.5°, 36.7°, 46.2°, and 56.1° (ref. 36) are weakly detected, as they could be masked by those obtained in the diffractograms of the prepared catalysts (Fig. 1a). The presence of niobium induced a substitution of Ti^{4+} with Nb^{5+}, which affected the crystallinity of the material. A niobium loading of up to 1% w/w led to a decrease in the FWHM of the 25° peak and an increase in crystallinity (Fig. 1b),[37,38] while for higher niobium loadings of up to 15% the amorphous phase became much more significant due to the collapse of the anatase structure (Fig. 1a).[39]

The thermogravimetric curves are similar for all samples, with the first mass loss occurring between 25 and 140 °C (Fig. 1c) corresponding to the elimination of physically adsorbed and chemisorbed water molecules.[40] The second step (140–350 °C) corresponds to the elimination of the weakly bound OH groups and the thermal decomposition of the organic part from the titanium and niobium precursors. The weight loss observed in the 350–700 °C range could correspond to the decomposition of the remaining Ti- and Nb-based compounds.[41] On the other hand, the formation of Nb–O–Ti bonds may be caused by the lower weight loss of 10% Ti–10% Nb/AC (44.4%) compared to 10% Ti/AC (52.55%).

The oxidation states of Ti and Nb and the relative surface composition were investigated using XPS analysis. The Ti 2p XPS spectrum of 10% Ti/AC consists of two components due to spin–orbit splitting, Ti $2p_{3/2}$ and Ti $2p_{1/2}$, which are observed at 458.7 eV and 464.5 eV, respectively (Fig. 1d and Table S1), confirming the 4+ oxidation state of Ti.[42] After the addition of niobium, no significant change was observed in the spectrum, confirming no change in the oxidation state of Ti and indicating a strong interaction between Nb and Ti, which was previously ascribed to Nb–O–Ti bond formation.[43] The Nb 3d XPS spectrum consists of two components due to spin–orbit splitting, Nb $3d_{5/2}$ and Nb $3d_{3/2}$, which are seen at 207.0 eV and 209.7 eV, respectively and are congruent with the 5+ oxidation state of Nb, likely as Nb_2O_5 oxide. No significant changes were seen in the position and FWHM of the peaks with increasing Nb content (Fig. 1e and Table S2). The O 1s spectrum was deconvoluted into three components (Fig. S3 and Table S3): the lowest-energy component found between 529.7 and 530 eV corresponds to the lattice oxygen in the metal oxide structure;[44,45] the one at

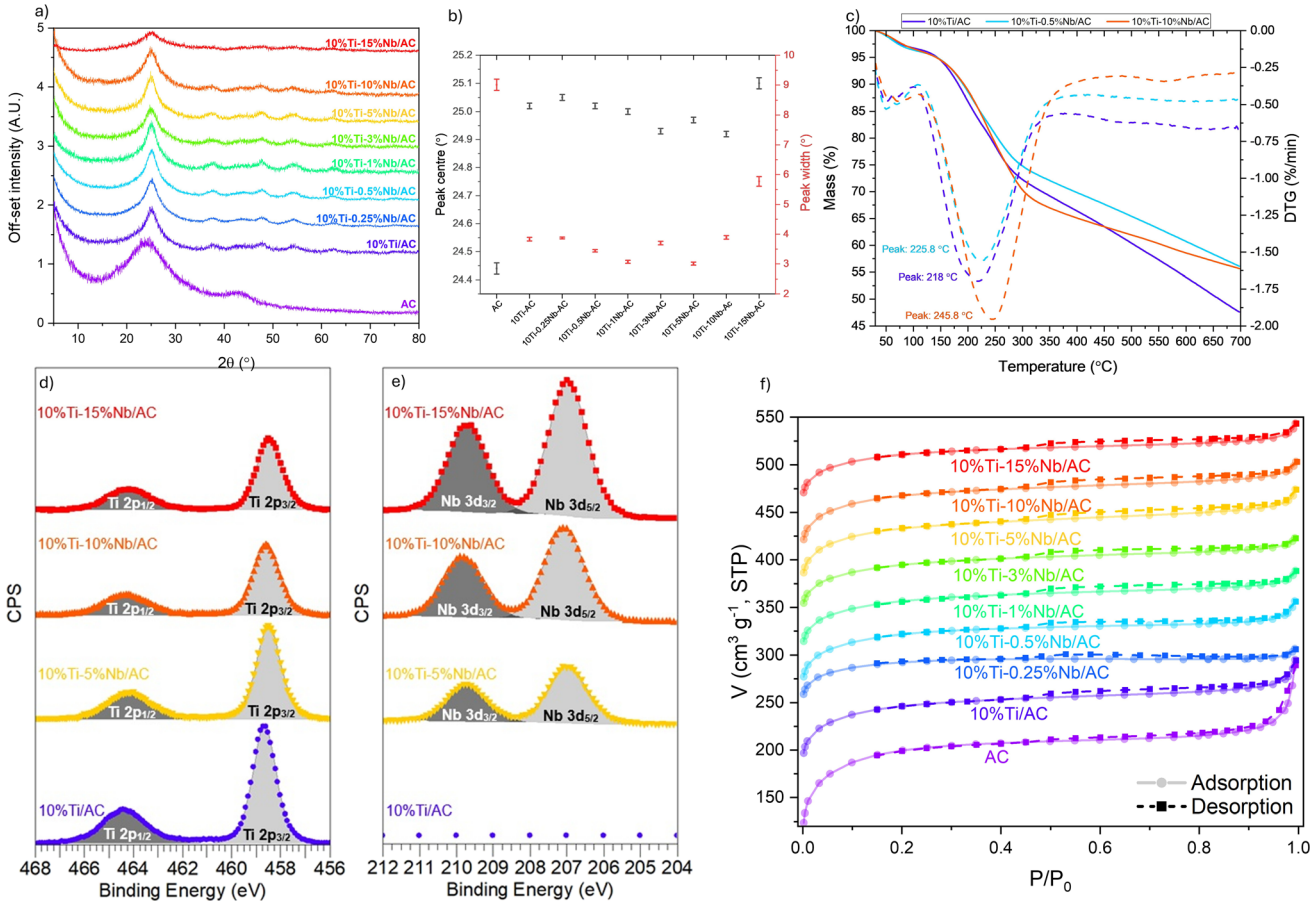

Fig. 1 (a) PXRD patterns of the catalysts; (b) variation of the peak centre and peak width of the primary peak in (a) (for more information about the data fitting, see Fig. S2); (c) TG and DTG curves; XPS analysis of the (d) Ti 2p and (e) Nb 3d spectra; (f) adsorption–desorption isotherms. Curves shown in (f) are shifted along the *y*-axis for better visibility.

~531 eV corresponds to the acidic bridging hydroxyl groups in the metal oxides[46] or to the adventitious hydroxyls of water,[47] while the last one is attributed to organic oxygen (bound to carbon atoms).[48] In our case, we postulate that the third component, appearing at higher B.E. values, corresponds to carbonate species, consistent with the observation of weak contributions on the C 1s spectrum near 286.0 eV and 288.0 eV, which are assigned to C–OH and C=O functional groups. Semiquantitative analysis shows that the gradual increase of the Nb/Ti ratio is consistent with the evolution of the nominal composition of niobium, while the surface O/(Ti + Nb) ratio remains relatively constant (Table S4).

The textural properties of AC changed after the incorporation of Nb and Ti, showing a decrease in specific surface (from 859 to 450 $m^2 g^{-1}$) and average pore size (from 6.8 to around 4 nm) (Table 1). Moreover, even after titanium and niobium impregnation, the AC retained the type IV isotherm (Fig. 1f),[49] regardless of the titanium or niobium loadings.

Sample morphology on the nanoscale level and the distribution of titanium and niobium on the AC surface were assessed by STEM-EDS mapping. The Nb and Ti particles showed no regular shape, with sizes up to 3 μm (Fig. 2a–e). The mapping showed that the distribution of C and (TiNb) is almost anti-correlated, although some C is present throughout the entire sample. The quantification of the EDS maps on the rich (TiNb) areas confirmed the presence of Nb species in all samples (average composition indicated in white in Fig. 2a–e). These observations are in relatively good agreement with XPS measurements, emphasising the segregation of TiO_2 and Nb_2O_5 rather than the build-up of Ti–O–Nb entities, which would correspond to a random distribution of Nb and Ti in the analysed area.

AFM imaging has been widely used to determine the particle size of 2D materials.[50] In agreement with XRD, the AFM images showed nanosized particles of niobium-doped titania for both 10% Ti–0.25% Nb/AC and 10% Ti–15% Nb/AC. For low Nb loading, the nanoparticles are in the range of 20–40 nm, while at higher loadings the nanoparticle sizes are up to 200 nm, which can be attributed to aggregation[51] (Fig. 2f–h). As can be noticed, the spherical shape of the particles was maintained irrespective of the amount of niobium added.

The presence of acid sites both in the presence and absence of titanium and niobium on the AC surface with different strengths was highlighted by NH_3-TPD measurements (Table 2 and Fig. S4). In agreement with the literature, the acid sites can be weak (desorption temperatures from 150 to 250 °C), medium (250 to 350 °C), and strong (350–600 °C).[52] Although an increase in the concentration of strong acid sites due to the presence of titanium was noticed, the increase was much more significant

Table 1 Textural characteristics of the investigated catalysts

Catalyst	Specific surface area ($m^2\ g^{-1}$)	Average pore size (nm)	Average pore volume ($cm^3\ g^{-1}$)
AC	859	6.8	0.19
10% Ti/AC	543	4.9	0.11
10% Ti–0.25% Nb/AC	527	4.2	0.08
10% Ti–0.5% Nb/AC	510	4.0	0.08
10% Ti–1% Nb/AC	489	4.0	0.09
10% Ti–3% Nb/AC	462	3.8	0.08
10% Ti–5% Nb/AC	513	4.4	0.1
10% Ti–10% Nb/AC	511	4.1	0.09
10% Ti–15% Nb/AC	450	4.4	0.08

with the addition of a small amount of niobia. We notice a linear correlation between the surface Nb/Ti ratio and the total amount of desorbed ammonia (Fig. S5). While the presence of titania led to an increase in the acidity as a result of Lewis acidity,[53] generating new Lewis and Brønsted acid sites, the addition of niobia led to an additional increase in the acidity.[51] On the other hand, an increase in niobium loading above 1% affected the stability of the anatase structure which led to the formation of an amorphous niobia–titania mixed oxide (Fig. 1a) justifying the minor increase in acidity compared to that obtained for 0.25% niobium loading (Table 2).[54]

3.2. Catalytic testing

As reported, titania shows low catalytic performance in the conversion of cellulose to value-added compounds.[55] Our results show low catalytic performance in terms of cellulose conversion and η_{LacA} of 10% Ti/AC (Fig. 3a), which agrees with previous reports.[53] Wattanapaphawong *et al.*[30] also reported low η_{LacA} (2.8% and 0.6%) for cellulose conversion over titania or niobia, respectively. The low catalytic activity of 10% Ti/AC can be attributed to the low acidity of titania.[56]

The addition of niobium along with titanium significantly increased the acidity of the material and η_{LacA} (from 1.6% over 10% Ti/AC to 14% over 10% Ti–0.5% Nb/AC). When varying the amount of Nb in the sample, a volcano plot-like trend is observed for both the cellulose conversion and η_{LacA} (Fig. 3a). Optimal parameters are observed at low Nb content (0.5–1% Nb) while subsequent increases in Nb loading have a detrimental effect on the overall catalytic activity. At low loadings, the niobia species are expected to be well-dispersed and isolated on the surface of the biochar support through Nb–O–C bonds. An increase in niobia loading also increases the number of Nb–O–

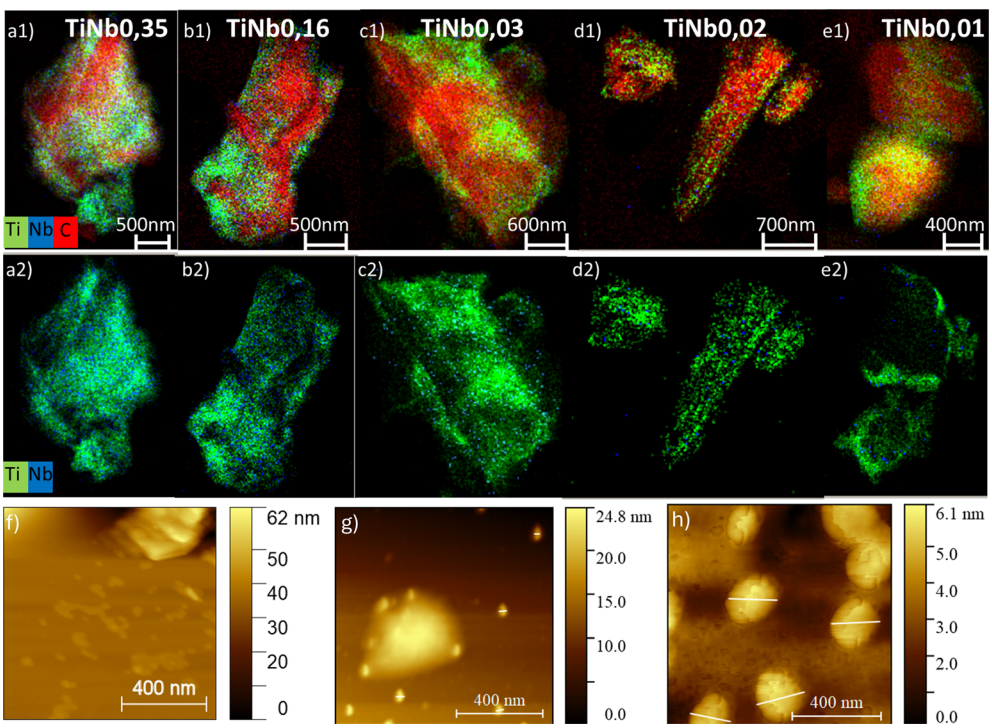

Fig. 2 (a)–(e) STEM-EDS mapping (top row: Ti, Nb, C; bottom row: Ti, Nb) for (a) 10% Ti–10% Nb/AC; (b) 10% Ti–5% Nb/AC; (c) 10% Ti–1% Nb/AC; (d) 10% Ti–0.5% Nb/AC; (e) 10% Ti–0.25% Nb/AC. The calculated average composition is shown in white. (f)–(h) AFM images of (f) AC, (g) 10% Ti–0.25% Nb/AC, and (h) 10% Ti–15% Nb/AC.

Table 2 The strength of acidic sites for AC supported and non-supported catalysts

Catalyst	μmol NH_3 per g				Acid site density (μmol m^{-2})
	Low	Medium	High	Total	
AC	227	176	1976	2379	2.76
10% Ti/AC	174	114	2350	2638	4.85
10% Ti–0.25% Nb/AC	202	18	3879	4099	7.77
10% Ti–0.5% Nb/AC	184	16	3904	4104	8.04
10% Ti–1% Nb/AC	90	39	3990	4119	8.42
10% Ti–3% Nb/AC	291	54	3972	4317	9.34
10% Ti–5% Nb/AC	249	62	4021	4332	8.44
10% Ti–10% Nb/AC	266	78	4121	4465	8.73
10% Ti–15% Nb/AC	111	102	4351	4564	10.14

Nb or Ti–O–Nb bridges due to the interaction between isolated species and their nearest neighbours,[51,57] which in turn lowers the catalytic activity. Therefore, catalytic performances were enhanced at low niobium loading due to the synergistic interaction between Brønsted and Lewis acid sites generated on the surface of the support as a result of the catalyst preparation. The η_{LacA} decrease with increased niobium loading is in line with STEM-EDS analysis that shows preferential segregation of TiO_2 and Nb_2O_5 on 10% Ti–5% Nb/AC.

The low catalytic activity of the samples with high niobium loadings can be attributed to the amorphisation of niobia and titania, as confirmed by the XRD analysis (Fig. 1a). An increase in Nb-loading leads to the amorphisation of niobia and the formation of saturated Nb species, whose catalytic activity is lower than that of unsaturated niobium from crystalline niobia.[58] A decrease in crystallite size as a result of Nb addition alongside Ti was highlighted in our previous study[59] and a positive correlation between anatase crystallite size and catalytic performance in the photo-degradation of phenol was reported by X. Wang *et al.*[60] Therefore, the behaviour of our catalysts in the conversion of cellulose to LacA as a function of the Nb loading is in agreement with literature data and the particle aggregation at 15% Nb loading (Fig. 2h) justifies the low catalytic activity of 10% Ti–15% Nb/AC (Fig. 3a).

The effectiveness of the 10% Ti–5% Nb/AC catalyst is related to parallel reactions involving fructose as a common intermediate product. Afterwards, undesired reaction pathways can lead to the ultimate formation of LevA promoted on Brønsted and Lewis acid sites. In this specific case, the acidic function

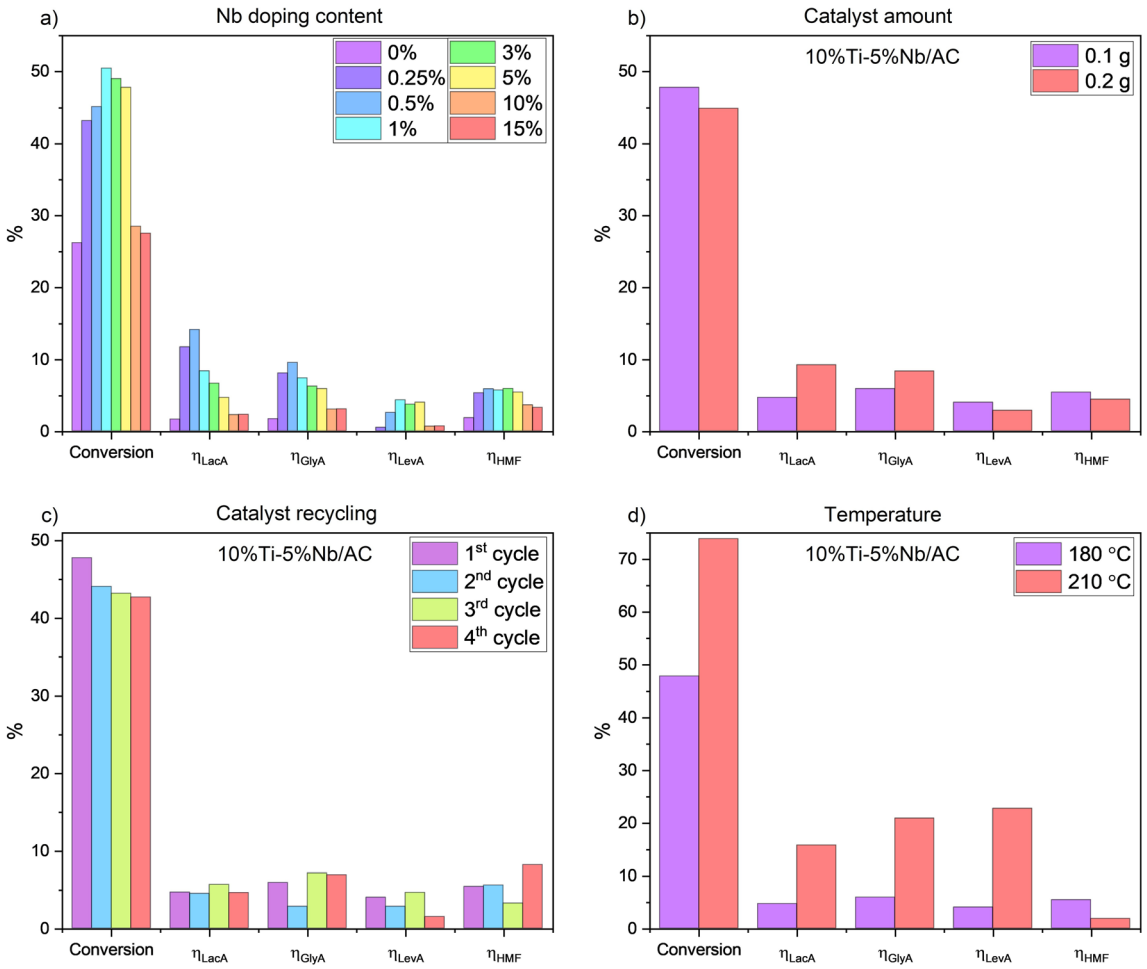

Fig. 3 Influence of different parameters on the catalytic activity of the catalyst: (a) niobium doping content; (b) amount of catalyst; (d) temperature. (c) Results of reusing the catalyst for four cycles.

would outperform the redox function of the catalyst. To a certain extent, such a trend is in agreement with our results, where the higher Nb loadings increased the acidity. This evolution is well illustrated in the particular case of 10% Ti–5% Nb/AC. Various experimental parameters were investigated, including the amount of the catalyst. As such, doubling the catalyst amount led to an enhancement of η_{LacA} from 4.6% to 9.2% (Fig. 3b). The correlative decrease in η_{LevA} at higher catalyst loadings could be attributed to humin formation through HMF aldol addition and condensation.[61]

Although most heterogeneous catalysts lose their Lewis acids in hydrolysis processes, the Lewis acidic nature of unsaturated Ti^{4+} and Nb^{5+} sites leads to a low interaction with water molecules and thus low hydration, which justifies the catalytic activity of niobia and titania in aqueous media.[62,63] On the surface of titania, there are both saturated (in TiO_6 octahedra) and unsaturated (in TiO_4 tetrahedra) titanium atoms, with the latter still acting as Lewis acid sites even in water. A similar behaviour was observed for Nb_2O_5, where some of the unsaturated NbO_4 tetrahedra maintain their Lewis acidity even in water.[63] Therefore, the Lewis acid sites in the TiO_4 and NbO_4 tetrahedra allowed the reusability of 10% Ti–5% Nb/AC for four catalytic cycles without any significant loss in catalytic activity (Fig. 3c). We attribute the slight decrease in the conversion to the formation of undissolved humins during the production of HMF,[64] which may block the conversion of residual cellulose.[65] To date, only a handful of studies reported the conversion of cellulose to LacA over titania or niobia catalysts, primarily due to their low catalytic activity. Wattanapaphawong *et al.* showed that niobia and titania led to $\eta_{LacA} < 5\%$.[30] An improvement in the catalytic performance of these oxides was noticed in our study by supporting niobium and titanium together on the activated biochar with trimodal (micro-, meso-, and macro-) porosity, which led to $\eta_{LacA} = 14\%$, for a low catalyst to cellulose mass ratio (1 : 5). The production of higher η_{LacA} from cellulose was reported in the literature, but it required harsher conditions (190 °C, 24 h, 50 MPa He) and a high catalyst (AlW) to cellulose mass ratio of 1 : 2.[66] Therefore, the improvement of catalytic performance of niobium and/or titanium-based materials in the production of LacA from cellulose remains a true challenge.

Increasing the temperature from 180 °C to 210 °C resulted in a much higher η_{LevA} compared to η_{LacA} and a higher cellulose conversion (Fig. 3d), which may be attributed to the water behaviour under subcritical conditions (100–374 °C), which in turn could influence the nature of the acid properties of biochar-supported catalysts. The high water density under subcritical conditions can generate Brønsted acidity by the adsorption of H^+ species on the surface of TiO_2, which encourages the use of TiO_2 materials in aqueous-phase biomass conversions.[67] Consequently, the increase in temperature was accompanied by an increase in the concentration of Brønsted acid sites, which in turn increased the conversion of cellulose to LevA. Similar results were also reported in our previous study.[34]

The diffraction lines corresponding to anatase were preserved for 10% Ti–5% Nb/AC tested at 180 °C and 210 °C. On the other hand, for 10% Ti–5% Nb/AC tested at 180 °C two additional peaks were noticed at 2θ values of 14.9° and 22.4°, as well as a shoulder at around 34.2°, corresponding to unreacted cellulose.[68] The absence of these peaks for the catalytic conversion at 210 °C could be due to the formation of hydrochar[69] (Fig. S6a). The distribution of niobium and titanium on the surface of the activated carbon for 10% Ti–5% Nb/AC was almost homogeneous before the reaction, as highlighted by SEM-EDS mapping (Fig. S6b). However, we noticed that the distribution was affected during the catalytic process (Fig. S6c and d). On the other hand, a decrease in the amount of niobium on the surface of carbon by increasing the working temperature from 180 °C to 210 °C was noticed (Fig. S6d). This effect was also confirmed by STEM-EDS analysis (Fig. S7). Although niobia shows high stability in water even at high temperatures, harsh conditions and long exposure time can affect its stability,[70] which is in agreement with our experimental results.

3.3. Influence of the textural properties of the support

The textural properties of the biochar that resulted from SCGs depend on the salts used in the chemical activation process. The biochar obtained using only $ZnCl_2$ (AC_{micro}) is microporous with high specific surface area,[31,71] while only using $LaCl_3$ results in a biochar (AC_{LaCl_3}) with low specific surface area. Similarly, the beneficial effect of $LaCl_3$ for the generation of large pores was previously reported[72] and confirmed by the increase in average pore size and volume in our control experiment (AC_{LaCl_3}). Our new approach showed that the addition of both $LaCl_3$ and $ZnCl_2$ leads to an activated biochar (AC) with trimodal (micro-, meso-, and macro-) porosity[73] (Fig. S8a) and a high specific surface (Table S5). Therefore, the generation of these new properties was the consequence of the synergistic effect between zinc and lanthanum chloride. The presence of these new pores is even more interesting as the activated biochar with only $ZnCl_2$ shows only micropores (Fig. S8b).

The 10% Ti–10% Nb/AC_{micro} catalyst was synthesised starting from AC_{micro}, allowing us to examine the impact of the support's textural properties. Adsorption–desorption isotherms confirm that the textural properties of the biochar were preserved after the Ti and Nb impregnation, with 10% Ti–10% Nb/AC showing the IV isotherm, while 10% Ti–10% Nb/AC_{micro} displays a type I isotherm (Fig. 4c and Table S5).

The textural properties of the biochar also influenced the crystallite size and the catalytic performance. The generation of meso- and macropores on the surface of the biochar as a result of $LaCl_3$ allowed an increase in crystallite size of niobium doped titania from 1.6 nm (AC_{micro}) to 2 nm (AC), which resulted in a narrowing of the FWHM of the primary peak from 5.1° (Fig. 4a2) to 3.9° (Fig. 4a1). Therefore, the formation of niobium-doped titania with different sizes depended on the size of the pores.[74] The XPS analysis of the Ti 2p and Nb 3d spectra shows no significant differences between the micro- and mesoporous catalysts (Fig. 4b).

Cellulose first interacts with the active sites on the exterior surface of the catalyst, where it depolymerises into oligomers and then into glucose. The access of these small molecules into the acidic centres is then facilitated by the meso- and macroporous structures.[75] Therefore, besides the niobium loading, the porosity also influences the catalytic activity. Dias *et al.*[76] reported the

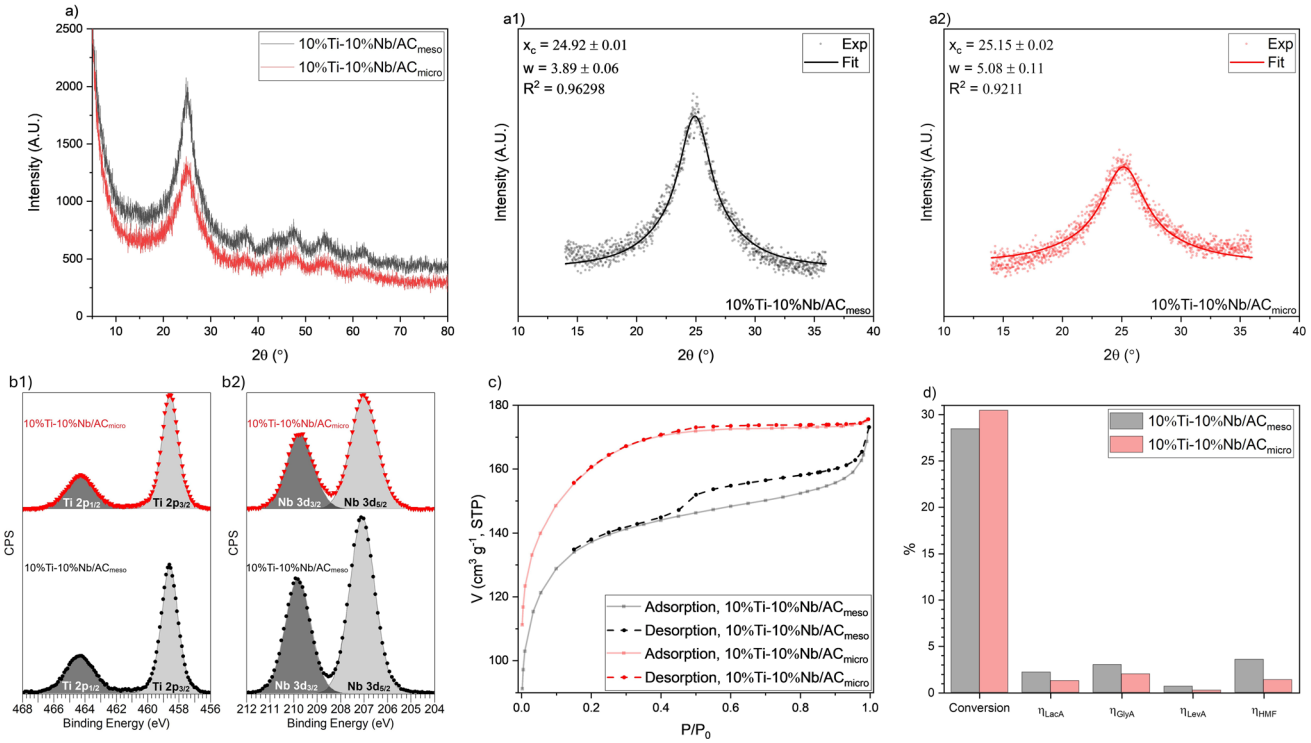

Fig. 4 Structural and catalytic comparison of the materials obtained with zinc(II) chloride, without lanthanum(III) chloride (AC_{micro}, red) and with zinc and lanthanum chloride (AC_{meso}, black). (a) Powder X-ray diffraction patterns. (a1)–(a2) The fitting of the primary peak. (b) (1) Ti 2p and (2) Nb 3d XPS spectra; (c) adsorption–desorption isotherms; (d) catalytic activity.

dehydration of xylose to furfural over meso- and microporous silica, with larger diameters of mesopores enhancing furfural yields. Herein, the dehydration of fructose to HMF over mesoporous biochar-supported nano titanium–niobium oxides led to an increase in η_{HMF} from 1.3 to 3.5% (Fig. 4d). On the other hand, lower catalytic performances of the microporous biochar-based acid catalysts can also be caused by mass transfer limitations characterised by a lower average pore size.[77]

4 Conclusions

We propose a new approach for the synthesis of biochars with different textural properties through the carbonisation of SCGs by using various ratios of lanthanum(III) and zinc(II) chlorides in the chemical activation process. When using an appropriate ratio between zinc and lanthanum chloride, a biochar with trimodal (micro-, meso-, and macro-) porosity and a high specific surface was obtained. The resulting biochars were then used to obtain biochar-supported nano-titanium–niobium oxides and the impact of the Nb loading on the catalytic performance of cellulose conversion to lactic acid was investigated. The presence of niobia and titania on the biochar surface was highlighted by XPS, XRD, SEM-EDS, and STEM-EDS. The high niobium loading led to a widening of the XRD peak at $2\theta = 25°$ and aggregation, as noticed by AFM analysis. The textural properties of the biochar influenced both crystallite size and catalytic performance, with large pores allowing the formation of larger crystallites. A significant improvement in the acidic properties of the AC upon the addition of titanium and niobium was highlighted by NH_3-TPD analysis.

As expected, the niobium-free catalyst shows the lowest catalytic activity and the lowest lactic acid yield (1.6%). Upon the addition of niobium, the activity increases, with the best lactic acid yield obtained for a niobium loading of 0.5% (14%). A further increase in Nb loading (up to 15%) caused a decrease in catalytic performances due to the collapse of the anatase structure. Increasing the reaction temperature to 210 °C during the catalytic test favours the production of levulinic acid. The biochar-supported nano-titanium–niobium oxides demonstrated good performances under hydrothermal conditions during three successive catalytic cycles for cellulose conversion into lactic acid with no significant loss in catalytic activity.

In conclusion, our work proves that the catalytic performance in the formation of lactic acid through the conversion of cellulose is affected by both the textural properties of the biochar support and the presence of niobia along with titania. The mesoporous structure enhances mass transfer and accessibility to active sites, while the cooccurrence of titania and niobia produces a synergistic interaction between Brønsted and Lewis acid sites, thus leading to improved catalytic performance in the conversion of cellulose to lactic acid. Furthermore, our work provides a general framework to synthesise novel mesoporous-biochar-supported catalysts.

Author contributions

V. A. N.: investigation, data curation, and writing-review and editing; M. M. M.: methodology and investigation; A. D.: methodology and writing-review and editing; C. E. S.: methodology and investigation; E. O.: investigation; E. B.: methodology;

D. C.: investigation; V. F.: investigation; F. P.: investigation; M. H.: investigation; P. G.: writing-review and editing, supervision, and funding acquisition; M. N. V.: conceptualization, methodology, validation, writing-original draft preparation, supervision, and funding acquisition.

Conflicts of interest

The authors declare that they have no financial interests.

Abbreviations

η_x	Yield of x
AC	Mesoporous biochar activated with both $LaCl_3$ and $ZnCl_2$
AC_{LaCl_3}	Biochar activated with $LaCl_3$
AC_{micro}	Biochar activated with $ZnCl_2$
AFM	Atomic force microscopy
GlycA	Glycolic acid
HMF	5-Hydroxymethylfurfural
HR-STEM	High-resolution scanning transmission electron microscopy
LacA	Lactic acid
LevA	Levulinic acid
NH_3-TPD	Ammonia temperature-programmed desorption
PXRD	Powder X-ray diffraction
SCGs	Spent coffee grounds
XPS	X-ray photoelectron spectroscopy

Data availability

The data used in this study are available from the corresponding authors upon reasonable request.

Supplementary information is available. See DOI: https://doi.org/10.1039/d5su00687b.

Acknowledgements

This work was supported by a grant of the Ministry of Research, Innovation and Digitalization, UEFISCDI project PN-III-P2-2.1-PED-2021-4171, Nr.634/2022 and the EU's NextGenerationEU instrument through the National Recovery and Resilience Plan of Romania – Pillar III-C9-I8, managed by the Ministry of Research, Innovation and Digitalization, within the project entitled "Advanced 3D printing for designer catalysts applied to biomass conversion", contract no. 760086/23.05.2023, code CF 43/14.11.2023.

References

1 R. AliAkbari, M. H. Ghasemi, N. Neekzad, E. Kowsari, S. Ramakrishna, M. Mehrali and Y. Marfavi, High value add bio-based low-carbon materials: conversion processes and circular economy, *J. Cleaner Prod.*, 2021, **293**, 126101, DOI: 10.1016/j.jclepro.2021.126101.

2 M. Kumar, S. K. Bhujbal, K. Kohli, R. Prajapati, B. K. Sharma, A. D. Sawarkar, K. Abhishek, S. Bolan, P. Ghosh, M. B. Kirkham, L. P. Padhye, A. Pandey, M. Vithanage and N. Bolan, A review on value-addition to plastic waste towards achieving a circular economy, *Sci. Total Environ.*, 2024, **921**, 171106, DOI: 10.1016/j.scitotenv.2024.171106.

3 A. Sudhaik, P. Raizada, T. Ahamad, S. M. Alshehri, V.-H. Nguyen, Q. Van Le, S. Thakur, V. K. Thakur, R. Selvasembian and P. Singh, Recent advances in cellulose supported photocatalysis for pollutant mitigation: a review, *Int. J. Biol. Macromol.*, 2023, **226**, 1284–1308, DOI: 10.1016/j.ijbiomac.2022.11.241.

4 Y. Cao, J. Wang, M. Kang and Y. Zhu, Efficient synthesis of ethylene glycol from cellulose over Ni–WO_3/SBA-15 catalysts, *J. Mol. Catal. A: Chem.*, 2014, **381**, 46–53, DOI: 10.1016/j.molcata.2013.10.002.

5 X. Zhang, D. Zhang, Z. Sun, L. Xue, X. Wang and Z. Jiang, Highly efficient preparation of HMF from cellulose using temperature-responsive heteropolyacid catalysts in cascade reaction, *Appl. Catal., B*, 2016, **196**, 50–56, DOI: 10.1016/j.apcatb.2016.05.019.

6 S. S. Chen, T. Maneerung, D. C. W. Tsang, Y. S. Ok and C.-H. Wang, Valorization of biomass to hydroxymethylfurfural, levulinic acid, and fatty acid methyl ester by heterogeneous catalysts, *Chem. Eng. J.*, 2017, **328**, 246–273, DOI: 10.1016/j.cej.2017.07.020.

7 A. A. Marianou, C. M. Michailof, A. Pineda, E. F. Iliopoulou, K. S. Triantafyllidis and A. A. Lappas, Effect of Lewis and Brønsted acidity on glucose conversion to 5-HMF and lactic acid in aqueous and organic media, *Appl. Catal., A*, 2018, **555**, 75–87, DOI: 10.1016/j.apcata.2018.01.029.

8 F.-F. Wang, J. Liu, H. Li, C.-L. Liu, R.-Z. Yang and W.-S. Dong, Conversion of cellulose to lactic acid catalyzed by erbium-exchanged montmorillonite K10, *Green Chem.*, 2015, **17**, 2455–2463, DOI: 10.1039/C4GC02131B.

9 Q. Zhang, Y. Cao, Z. Xu, H. Lei, X. Duan, J. H. Clark and D. C. W. Tsang, Manganese-Biochar Catalyst for Sustainable Glycolic Acid Production from Biomass-Derived Glucose and Oligosaccharides, *ACS Sustainable Chem. Eng.*, 2024, **12**, 16423–16433, DOI: 10.1021/acssuschemeng.4c06938.

10 X. Lei, F.-F. Wang, C.-L. Liu, R.-Z. Yang and W.-S. Dong, One-pot catalytic conversion of carbohydrate biomass to lactic acid using an $ErCl_3$ catalyst, *Appl. Catal., A*, 2014, **482**, 78–83, DOI: 10.1016/j.apcata.2014.05.029.

11 S. Li, W. Deng, Y. Li, Q. Zhang and Y. Wang, Catalytic conversion of cellulose-based biomass and glycerol to lactic acid, *J. Energy Chem.*, 2019, **32**, 138–151, DOI: 10.1016/j.jechem.2018.07.012.

12 W. Dong, Z. Shen, B. Peng, M. Gu, X. Zhou, B. Xiang and Y. Zhang, Selective Chemical Conversion of Sugars in Aqueous Solutions without Alkali to Lactic Acid over a Zn-Sn-Beta Lewis Acid-Base Catalyst, *Sci. Rep.*, 2016, **6**, 26713, DOI: 10.1038/srep26713.

13 A. A. Marianou, C. C. Michailof, D. Ipsakis, K. Triantafyllidis and A. A. Lappas, Cellulose conversion into lactic acid over

supported HPA catalysts, *Green Chem.*, 2019, **21**, 6161–6178, DOI: 10.1039/C9GC02622C.
14 X. Yan, F. Jin, K. Tohji, A. Kishita and H. Enomoto, Hydrothermal conversion of carbohydrate biomass to lactic acid, *AIChE J.*, 2010, **56**, 2727–2733, DOI: 10.1002/aic.12193.
15 F.-F. Wang, H.-Z. Wu, H.-F. Ren, C.-L. Liu, C.-L. Xu and W.-S. Dong, Er/β-zeolite-catalyzed one-pot conversion of cellulose to lactic acid, *J. Porous Mater.*, 2017, **24**, 697–706, DOI: 10.1007/s10934-016-0306-9.
16 S. Zhang, F. Jin, J. Hu and W. Zhang, Role of metallic Zn, Ni and activated carbon additives in improving the hydrothermal conversion of glucose into lactic acid: improving the effect of Zn, Ni and activated carbon on lactic acid yield, *J. Chem. Technol. Biotechnol.*, 2017, **92**, 1046–1052, DOI: 10.1002/jctb.5080.
17 M. S. Holm, S. Saravanamurugan and E. Taarning, Conversion of Sugars to Lactic Acid Derivatives Using Heterogeneous Zeotype Catalysts, *Science*, 2010, **328**, 602–605, DOI: 10.1126/science.1183990.
18 M. Xia, Z. Shen, S. Xiao, M. Gu and Y. Zhang, Synergistic effects of bimetals and hierarchical structures in Mg–Sn-Beta-H zeolites for lactic acid synthesis from biomass-derived carbohydrates, *Catal. Sci. Technol.*, 2023, **13**, 3974–3986, DOI: 10.1039/D3CY00471F.
19 Y. Cui, J. Li, Z. Liu, H. Yu, D. Ding and J. Wang, Alkali etching-free synthesis of hierarchical Zr-BEA zeolite as a robust catalyst for the efficient production of lactic acid from carbohydrates, *Microporous Mesoporous Mater.*, 2023, **360**, 112737, DOI: 10.1016/j.micromeso.2023.112737.
20 A. M. Mylin, S. I. Levytska, M. E. Sharanda and V. V. Brei, Selective conversion of dihydroxyacetone–ethanol mixture into ethyl lactate over amphoteric ZrO_2–TiO_2 catalyst, *Catal. Commun.*, 2014, **47**, 36–39, DOI: 10.1016/j.catcom.2014.01.004.
21 K. Lin, L. Li, B. F. Sels, P. A. Jacobs and P. P. Pescarmona, Titanosilicate beads as versatile catalysts for the conversion of trioses to lactates and for the epoxidation of alkenes, *Catal. Today*, 2011, **173**, 89–94, DOI: 10.1016/j.cattod.2011.03.055.
22 T. Okuhara, Water-Tolerant Solid Acid Catalysts, *Chem. Rev.*, 2002, **102**, 3641–3666, DOI: 10.1021/cr0103569.
23 X. Wang, Y. Song, L. Huang, H. Wang, C. Huang and C. Li, Tin modified Nb_2O_5 as an efficient solid acid catalyst for the catalytic conversion of triose sugars to lactic acid, *Catal. Sci. Technol.*, 2019, **9**, 1669–1679, DOI: 10.1039/C9CY00257J.
24 S. M. Coman, M. Verziu, A. Tirsoaga, B. Jurca, C. Teodorescu, V. Kuncser, V. I. Parvulescu, G. Scholz and E. Kemnitz, NbF_5–AlF_3 Catalysts: Design, Synthesis, and Application in Lactic Acid Synthesis from Cellulose, *ACS Catal.*, 2015, **5**, 3013–3026, DOI: 10.1021/acscatal.5b00282.
25 M. Verziu, M. Serano, B. Jurca, V. I. Parvulescu, S. M. Coman, G. Scholz and E. Kemnitz, Catalytic features of Nb-based nanoscopic inorganic fluorides for an efficient one-pot conversion of cellulose to lactic acid, *Catal. Today*, 2018, **306**, 102–110, DOI: 10.1016/j.cattod.2017.02.051.
26 A. Rana, S. Sonu, V. Soni, A. Chawla, A. Sudhaik, P. Raizada, T. Ahamad, P. Thakur, S. Thakur and P. Singh, Novel S-scheme derived Mo–Bi_2WO_6/WO_3/Biochar composite for photocatalytic removal of Methylene Blue dye, *J. Phys. Chem. Solids*, 2025, **196**, 112385, DOI: 10.1016/j.jpcs.2024.112385.
27 L. C. A. Oliveira, E. Pereira, I. R. Guimaraes, A. Vallone, M. Pereira, J. P. Mesquita and K. Sapag, Preparation of activated carbons from coffee husks utilizing $FeCl_3$ and $ZnCl_2$ as activating agents, *J. Hazard. Mater.*, 2009, **165**, 87–94, DOI: 10.1016/j.jhazmat.2008.09.064.
28 T. E. Rufford, D. Hulicova-Jurcakova, Z. Zhu and G. Q. Lu, Nanoporous carbon electrode from waste coffee beans for high performance supercapacitors, *Electrochem. Commun.*, 2008, **10**, 1594–1597, DOI: 10.1016/j.elecom.2008.08.022.
29 R. Campbell, B. Xiao and C. Mangwandi, Production of activated carbon from spent coffee grounds (SCG) for removal of hexavalent chromium from synthetic wastewater solutions, *J. Environ. Manage.*, 2024, **366**, 121682, DOI: 10.1016/j.jenvman.2024.121682.
30 P. Wattanapaphawong, P. Reubroycharoen and A. Yamaguchi, Conversion of cellulose into lactic acid using zirconium oxide catalysts, *RSC Adv.*, 2017, **7**, 18561–18568, DOI: 10.1039/C6RA28568F.
31 M. Verziu, M. Marin, A. Dumitru, V. Oprisan-Fruth, J. Pandee-Cusu and S.-E. Lazar, Process for the catalytic production of activated mesoporous carbon from biomass waste, A/00257, 2023.
32 N. Wetchakun, B. Incessungvorn, K. Wetchakun and S. Phanichphant, Influence of calcination temperature on anatase to rutile phase transformation in TiO_2 nanoparticles synthesized by the modified sol–gel method, *Mater. Lett.*, 2012, **82**, 195–198, DOI: 10.1016/j.matlet.2012.05.092.
33 M. Watanabe, Y. Aizawa, T. Iida, R. Nishimura and H. Inomata, Catalytic glucose and fructose conversions with TiO_2 and ZrO_2 in water at 473K: relationship between reactivity and acid–base property determined by TPD measurement, *Appl. Catal., A*, 2005, **295**, 150–156, DOI: 10.1016/j.apcata.2005.08.007.
34 S. Avramescu, C. D. Ene, M. Ciobanu, J. Schnee, F. Devred, C. Bucur, E. Vasile, L. Colaciello, R. Richards, E. M. Gaigneaux and M. N. Verziu, Nanocrystalline rhenium-doped TiO_2: an efficient catalyst in the one-pot conversion of carbohydrates into levulinic acid. The synergistic effect between Brønsted and Lewis acid sites, *Catal. Sci. Technol.*, 2022, **12**, 167–180, DOI: 10.1039/D1CY01450A.
35 L. Ye, J. Mao, J. Liu, Z. Jiang, T. Peng and L. Zan, Synthesis of anatase TiO_2 nanocrystals with {101}, {001} or {010} single facets of 90% level exposure and liquid-phase photocatalytic reduction and oxidation activity orders, *J. Mater. Chem. A*, 2013, **1**, 10532, DOI: 10.1039/c3ta11791j.
36 M. Joya, J. Barba Ortega, A. Raba Paez, J. Da Silva Filho and P. Cavalcante Freire, Synthesis and Characterization of Nano-Particles of Niobium Pentoxide with Orthorhombic Symmetry, *Metals*, 2017, **7**, 142, DOI: 10.3390/met7040142.

37 Z. Liu, Y. Zheng, T. Gao, J. Zhang, X. Sun and G. Zhou, Fabrication of anatase TiO_2 tapered tetragonal nanorods with designed {100}, {001} and {101} facets for enhanced photocatalytic H_2 evolution, *Int. J. Hydrogen Energy*, 2017, **42**, 21775–21785, DOI: 10.1016/j.ijhydene.2017.07.067.

38 X. Wang, D. Zhang, Q. Xiang, Z. Zhong and Y. Liao, Review of Water-Assisted Crystallization for TiO_2 Nanotubes, *Nano-Micro Lett.*, 2018, **10**, 77, DOI: 10.1007/s40820-018-0230-4.

39 S. Li, Q. Xu, E. Uchaker, X. Cao and G. Cao, Comparison of amorphous, pseudohexagonal and orthorhombic Nb_2O_5 for high-rate lithium ion insertion, *CrystEngComm*, 2016, **18**, 2532–2540, DOI: 10.1039/C5CE02069G.

40 C.-Y. Wu, K.-J. Tu, J.-P. Deng, Y.-S. Lo and C.-H. Wu, Markedly Enhanced Surface Hydroxyl Groups of TiO_2 Nanoparticles with Superior Water-Dispersibility for Photocatalysis, *Materials*, 2017, **10**, 566, DOI: 10.3390/ma10050566.

41 B. Fazlioglu-Yalcin, M. Hilse and R. Engel-Herbert, Thermogravimetric study of metal–organic precursors and their suitability for hybrid molecular beam epitaxy, *J. Mater. Res.*, 2024, **39**, 436–448, DOI: 10.1557/s43578-023-01237-w.

42 H. Wang, X. Yuan, Y. Wu, G. Zeng, X. Chen, L. Leng, Z. Wu, L. Jiang and H. Li, Facile synthesis of amino-functionalized titanium metal-organic frameworks and their superior visible-light photocatalytic activity for Cr(VI) reduction, *J. Hazard. Mater.*, 2015, **286**, 187–194, DOI: 10.1016/j.jhazmat.2014.11.039.

43 E. Uyanga, A. Gibaud, P. Daniel, D. Sangaa, G. Sevjidsuren, P. Altantsog, T. Beuvier, C. H. Lee and A. M. Balagurov, Structural and vibrational investigations of Nb-doped TiO_2 thin films, *Mater. Res. Bull.*, 2014, **60**, 222–231, DOI: 10.1016/j.materresbull.2014.08.035.

44 B. Bharti, S. Kumar, H.-N. Lee and R. Kumar, Formation of oxygen vacancies and Ti^{3+} state in TiO_2 thin film and enhanced optical properties by air plasma treatment, *Sci. Rep.*, 2016, **6**, 32355, DOI: 10.1038/srep32355.

45 L. Yang, P. Gao, J. Lu, W. Guo, Z. Zhuang, Q. Wang, W. Li and Z. Feng, Mechanism analysis of Au, Ru noble metal clusters modified on TiO_2 (101) to intensify overall photocatalytic water splitting, *RSC Adv.*, 2020, **10**, 20654–20664, DOI: 10.1039/D0RA01996H.

46 K. Lau, F. Niemann, K. Abdiaziz, M. Heidelmann, Y. Yang, Y. Tong, M. Fechtelkord, T. C. Schmidt, A. Schnegg, R. K. Campen, B. Peng, M. Muhler, S. Reichenberger and S. Barcikowski, Differentiating between Acidic and Basic Surface Hydroxyls on Metal Oxides by Fluoride Substitution: A Case Study on Blue TiO_2 from Laser Defect Engineering, *Angew. Chem., Int. Ed.*, 2023, **62**, e202213968, DOI: 10.1002/anie.202213968.

47 H. Idriss, On the wrong assignment of the XPS O1s signal at 531–532 eV attributed to oxygen vacancies in photo- and electro-catalysts for water splitting and other materials applications, *Surf. Sci.*, 2021, **712**, 121894, DOI: 10.1016/j.susc.2021.121894.

48 G. Beamson and D. Briggs, High Resolution XPS of Organic Polymers: The Scienta ESCA300 Database, *J. Chem. Educ.*, 1993, **70**, A25, DOI: 10.1021/ed070pA25.5.

49 M. M. Rahman, A. Z. Shafiullah, A. Pal, M. A. Islam, I. Jahan and B. B. Saha, Study on Optimum IUPAC Adsorption Isotherm Models Employing Sensitivity of Parameters for Rigorous Adsorption System Performance Evaluation, *Energies*, 2021, **14**, 7478, DOI: 10.3390/en14227478.

50 Á. Mechler, J. Kopniczky, J. Kokavecz, A. Hoel, C.-G. Granqvist and P. Heszler, Anomalies in nanostructure size measurements by AFM, *Phys. Rev. B: Condens. Matter Mater. Phys.*, 2005, **72**, 125407, DOI: 10.1103/PhysRevB.72.125407.

51 H. Jiao, X. Zhao, C. Lv, Y. Wang, D. Yang, Z. Li and X. Yao, Nb_2O_5-γ-Al_2O_3 nanofibers as heterogeneous catalysts for efficient conversion of glucose to 5-hydroxymethylfurfural, *Sci. Rep.*, 2016, **6**, 34068, DOI: 10.1038/srep34068.

52 D. Liu, P. Yuan, H. Liu, J. Cai, D. Tan, H. He, J. Zhu and T. Chen, Quantitative characterization of the solid acidity of montmorillonite using combined FTIR and TPD based on the NH_3 adsorption system, *Appl. Clay Sci.*, 2013, **80–81**, 407–412, DOI: 10.1016/j.clay.2013.07.006.

53 X. Gao and I. E. Wachs, Titania–silica as catalysts: molecular structural characteristics and physico-chemical properties, *Catal. Today*, 1999, **51**, 233–254, DOI: 10.1016/S0920-5861(99)00048-6.

54 R. Radhakrishnan, J. Wu, S. Jaenicke and G. K. Chuah, Effects of Acidity and Pore Size Constraints on Supported Niobium Oxide Catalysts for the Selective Formation of Glycerol Monolaurate, *ChemCatChem*, 2011, **3**, 761–770, DOI: 10.1002/cctc.201000300.

55 H. Lin, J. Strull, Y. Liu, Z. Karmiol, K. Plank, G. Miller, Z. Guo and L. Yang, High yield production of levulinic acid by catalytic partial oxidation of cellulose in aqueous media, *Energy Environ. Sci.*, 2012, **5**, 9773, DOI: 10.1039/c2ee23225a.

56 R. M. De Almeida, N. J. A. De Albuquerque, F. T. C. Souza and S. M. P. Meneghetti, Catalysts based on TiO_2 anchored with MoO_3 or SO_4^{2-} for conversion of cellulose into chemicals, *Catal. Sci. Technol.*, 2016, **6**, 3137–3142, DOI: 10.1039/C5CY01711D.

57 J. Mohd Ekhsan, S. L. Lee and H. Nur, Niobium oxide and phosphoric acid impregnated silica–titania as oxidative-acidic bifunctional catalyst, *Appl. Catal., A*, 2014, **471**, 142–148, DOI: 10.1016/j.apcata.2013.11.041.

58 L. Oliveira, M. Pereira, A. Pacheli Heitman, J. Filho, C. Oliveira and M. Ziolek, Niobium: The Focus on Catalytic Application in the Conversion of Biomass and Biomass Derivatives, *Molecules*, 2023, **28**, 1527, DOI: 10.3390/molecules28041527.

59 C. E. Stavarache, A. Khosravi, M. M. Marin, J. Pandele-Cusu, S. E. Lazar, F. Papa, V. Fruth, D. Culita, N. I. Cristea, S. Karakoulia, K. Triantafyllidis and M. N. Verziu, Catalytic synthesis of lactic acid from cellulose over easily-prepared niobium-doped titania by solution combustion synthesis, *Biomass Bioenergy*, 2025, **194**, 107687, DOI: 10.1016/j.biombioe.2025.107687.

60 X. Wang, L. Sø, R. Su, S. Wendt, P. Hald, A. Mamakhel, C. Yang, Y. Huang, B. B. Iversen and F. Besenbacher, The influence of crystallite size and crystallinity of anatase nanoparticles on the photo-degradation of phenol, *J. Catal.*, 2014, **310**, 100–108, DOI: 10.1016/j.jcat.2013.04.022.

61 S. S. Joshi, A. D. Zodge, K. V. Pandare and B. D. Kulkarni, Efficient Conversion of Cellulose to Levulinic Acid by Hydrothermal Treatment Using Zirconium Dioxide as a Recyclable Solid Acid Catalyst, *Ind. Eng. Chem. Res.*, 2014, **53**, 18796–18805, DOI: 10.1021/ie5011838.

62 K. Nakajima, Y. Baba, R. Noma, M. Kitano, J. N. Kondo, S. Hayashi and M. Hara, $Nb_2O_5 \cdot nH_2O$ as a Heterogeneous Catalyst with Water-Tolerant Lewis Acid Sites, *J. Am. Chem. Soc.*, 2011, **133**, 4224–4227, DOI: 10.1021/ja110482r.

63 K. Nakajima, R. Noma, M. Kitano and M. Hara, Titania as an Early Transition Metal Oxide with a High Density of Lewis Acid Sites Workable in Water, *J. Phys. Chem. C*, 2013, **117**, 16028–16033, DOI: 10.1021/jp404523r.

64 I. Delidovich, K. Leonhard and R. Palkovits, Cellulose and hemicellulose valorisation: an integrated challenge of catalysis and reaction engineering, *Energy Environ. Sci.*, 2014, **7**, 2803, DOI: 10.1039/C4EE01067A.

65 W. Yan, Q. Guan and F. Jin, Catalytic conversion of cellulosic biomass to harvest high-valued organic acids, *iScience*, 2023, **26**, 107933, DOI: 10.1016/j.isci.2023.107933.

66 F. Chambon, F. Rataboul, C. Pinel, A. Cabiac, E. Guillon and N. Essayem, Cellulose hydrothermal conversion promoted by heterogeneous Brønsted and Lewis acids: remarkable efficiency of solid Lewis acids to produce lactic acid, *Appl. Catal., B*, 2011, **105**, 171–181, DOI: 10.1016/j.apcatb.2011.04.009.

67 P. Sudarsanam, H. Li and T. V. Sagar, TiO_2-Based Water-Tolerant Acid Catalysis for Biomass-Based Fuels and Chemicals, *ACS Catal.*, 2020, **10**, 9555–9584, DOI: 10.1021/acscatal.0c01680.

68 K. S. Salem, N. K. Kasera, M. A. Rahman, H. Jameel, Y. Habibi, S. J. Eichhorn, A. D. French, L. Pal and L. A. Lucia, Comparison and assessment of methods for cellulose crystallinity determination, *Chem. Soc. Rev.*, 2023, **52**, 6417–6446, DOI: 10.1039/D2CS00569G.

69 Y. Lin, H. Xu, Y. Gao and X. Zhang, Preparation and characterization of hydrochar-derived activated carbon from glucose by hydrothermal carbonization, *Biomass Convers. Biorefin.*, 2023, **13**, 3785–3796, DOI: 10.1007/s13399-021-01407-y.

70 D. Ding, J. Wang, J. Xi, X. Liu, G. Lu and Y. Wang, High-yield production of levulinic acid from cellulose and its upgrading to γ-valerolactone, *Green Chem.*, 2014, **16**, 3846, DOI: 10.1039/C4GC00737A.

71 A. Namane, A. Mekarzia, K. Benrachedi, N. Belhanechebensemra and A. Hellal, Determination of the adsorption capacity of activated carbon made from coffee grounds by chemical activation with ZnCl and HPO, *J. Hazard. Mater.*, 2005, **119**, 189–194, DOI: 10.1016/j.jhazmat.2004.12.006.

72 A. K. Tolkou, S. Trikalioti, O. Makrogianni, M. Xanthopoulou, E. A. Deliyanni, I. A. Katsoyiannis and G. Z. Kyzas, Chromium(VI) Removal from Water by Lanthanum Hybrid Modified Activated Carbon Produced from Coconut Shells, *Nanomaterials*, 2022, **12**, 1067, DOI: 10.3390/nano12071067.

73 A. Liu, C. Mollart, A. Trewin, X. Fan and C. H. Lau, Photo-Modulating CO_2 Uptake of Hypercross-linked Polymers Upcycled from Polystyrene Waste, *ChemSusChem*, 2023, **16**, e202300019, DOI: 10.1002/cssc.202300019.

74 S. Perathoner, P. Lanzafame, R. Passalacqua, G. Centi, R. Schlögl and D. S. Su, Use of mesoporous SBA-15 for nanostructuring titania for photocatalytic applications, *Microporous Mesoporous Mater.*, 2006, **90**, 347–361, DOI: 10.1016/j.micromeso.2005.10.024.

75 S. She, L. P. P. Sukma, M. Peng, H. Shirai, Y. Suzuki, K. Kamiya and E. W. Qian, Hierarchically structured macro-mesoporous carbon catalysts for saccharification of cellulose, *Green Carbon*, 2025, **3**, 148–157, DOI: 10.1016/j.greenca.2024.11.006.

76 A. Dias, M. Pillinger and A. Valente, Dehydration of xylose into furfural over micro-mesoporous sulfonic acid catalysts, *J. Catal.*, 2005, **229**, 414–423, DOI: 10.1016/j.jcat.2004.11.016.

77 A. Taguchi and F. Schüth, Ordered mesoporous materials in catalysis, *Microporous Mesoporous Mater.*, 2005, **77**, 1–45, DOI: 10.1016/j.micromeso.2004.06.030.